Journal of Materials Chemistry A

ROYAL SOCIETY OF CHEMISTRY

PAPER

View Article Online
View Journal | View Issue

Cite this: J. Mater. Chem. A, 2025, 13, 26448

Highly conductive LiH_2PO_4-based solid electrolyte at intermediate temperatures through a polymerization-hydrolysis treatment†

Ke Xu,[a] Keisuke Obata,[a] Takaaki Suzuki,[b] Kazuya Yamaguchi,[b] Masao Katayama[a] and Kazuhiro Takanabe *[a]

Received 10th February 2025
Accepted 1st July 2025

DOI: 10.1039/d5ta01056j

rsc.li/materials-a

Establishing expandable solid electrolytes with high ionic conductivity at approximately 200 °C remains a significant challenge for various electrocatalytic applications. In this study, we developed a self-standing electrolyte membrane composed of H_3PO_4-containing LiH_2PO_4 and a quartz fiber (QF) matrix using a unique polymerization-hydrolysis (PH) synthesis method. We used a simple mixture of LiH_2PO_4 and H_3PO_4 as the precursor, and heating-induced phosphate polymerization resulted in a unique glassy sol formation that could be reshaped easily. Upon hydrolysis pretreatment with polyphosphate, LiH_2PO_4 was formed, and the electrolyte membrane exhibited high ionic conductivity. We optimized the infiltrating amount of H_3PO_4 to vary the maximum conductivity of the electrolyte. We conducted conductivity measurements under diverse temperatures and water humidities to determine the operating conditions for the electrolyte membrane. The LiH_2PO_4-based membrane maintained high conductivity (21–28 mS cm^{-1}) over a broad and comparatively low temperature range (100–200 °C) when supplied with water vapor. It is hypothesized that a phase containing H_2O and H_3PO_4 is formed at the interface between the LiH_2PO_4 particles, which contributes to the high conductivity. The scalability of the present fabrication method was confirmed by successfully forming a 100 mm Φ QF sheet displaying uniform conductivities through the sheet.

Introduction

Electrochemical devices typically consist of an anode and a cathode separated by an electrolyte to perform reactions. The electrolyte forms an ionic circuit between the anode and the cathode, and its conductivity significantly impacts ohmic voltage loss in electrochemical devices. The electrolyte's operating temperature and the resultant environment also affect reaction kinetics and applicable materials. Solid-state proton-conducting electrolytes operating at intermediate temperatures (*i.e.*, 100–300 °C) demonstrate numerous benefits for applications such as fuel cells and electrolyzers.[1–7] Operating at intermediate temperatures simplifies water and waste heat management, improves electrode kinetics, and enables the development of alternative electrocatalysts with enhanced activity.[8] Several types of materials have been reported as intermediate-temperature electrolytes, including superprotonic solid acids such as CsH_2PO_4,[9,10] inorganic acid-doped polymers such as phosphoric acid-polybenzimidazole (PA-PBI),[11,12] and tetravalent metal pyrophosphates such as SnP_2O_7.[3,13]

Typically, many solid acids suitable for electrolyte purposes consist of alkali metals and tetrahedral oxyanions linked together by hydrogen bonds ($M_xH_y(AO_4)_z$, where M = Cs, Rb, K, Li, or NH_4; A = S, Se, P, or As). These materials exhibit high proton conductivities at elevated temperatures but become insulating below certain temperatures.[14,15] This high conductivity is often attributed to a superprotonic phase transition (*e.g.*, CsH_2PO_4 transitioning from a monoclinic to a cubic phase at 230 °C), where the rearranged lattice allows protons to hop between oxyanions.[9,16–18] In contrast, some researchers have reported conductivity enhancement due to thermal decomposition. In this scenario, the water generated by the decomposition reaction dissolves a surface portion of the salt, providing protons to be conducted through the water embedded in the hygroscopic solid acids.[19–22] Inorganic acid-doped polymers (*e.g.*, H_3PO_4-doped PBI) typically function below 200 °C, where proton conduction mainly depends on the inorganic acid molecules and their interactions with the polymer matrix.[23] Inorganic oxides or phosphates (*e.g.*, SiO_2, SiP_2O_7, $Zr(HPO_4)$, and $Ce(HPO_4)_2$) are often added to electrolyte membranes to provide additional proton transport pathways or to improve water retention.[24–26] Metal pyrophosphates (MP_2O_7, where M = Sn, Ti, Si, Zr, Ce) have been studied owing to their high proton

[a]Department of Chemical System Engineering, School of Engineering, The University of Tokyo, Tokyo, 113-8656, Japan. E-mail: takanabe@chemsys.t.u-tokyo.ac.jp
[b]Department of Applied Chemistry, School of Engineering, The University of Tokyo, Tokyo, 113-8656, Japan

† Electronic supplementary information (ESI) available. See DOI: https://doi.org/10.1039/d5ta01056j

conductivity at intermediate temperatures and low humidity conditions.[27] A significant enhancement in proton conductivity can be achieved through the partial substitution of tetravalent metals with lower-valence metals (*e.g.*, Al^{3+} and In^{3+}).[3,28] However, some reports associate the high conductivity of metal pyrophosphates in the presence of a phosphoric acid-rich liquid phase at grain boundaries between solid phosphate particles.[29] In recent years, novel intermediate-temperature electrolytes have been developed. For example, Omata *et al.* reported proton-conducting phosphate glass electrolytes, such as $H_5Si_2P_9O_{29}$, synthesized using the alkali-proton substitution (APS) method, which can operate at around 280 °C.[30,31]

Despite decades of development, intermediate-temperature electrolytes still require improvements in conductivity and stability. Broadening the application temperature range of solid acid electrolytes poses a significant challenge. Solid acids have garnered considerable attention since Haile *et al.* successfully applied $CsHSO_4$ and CsH_2PO_4 solid acids to fuel cell systems at 160 °C and 250 °C, respectively, illustrating their potential for use in intermediate-temperature electrochemical devices.[1,2] However, as noted, solid acids lose their high conductivity below certain temperatures, limiting their application range. Consequently, many studies have focused on augmenting the solid acid conductivity at lower temperatures. Commonly used additives, such as oxides and pyrophosphates (*e.g.*, SiO_2, TiO_2, ZrO_2, and SiP_2O_7), serve as matrix materials for solid acids and can enhance electrolyte conductivity over a broad temperature range by generating disordered phases between the solid acid and the matrix.[32–35] For instance, although CsH_2PO_4 alone demonstrates high conductivity only above 230 °C, CsH_2PO_4 mixed with a SiP_2O_7 matrix maintains high conductivity down to 150 °C. It has been suggested that $CsH_5(PO_4)_2$, which is formed at the CsH_2PO_4 and SiP_2O_7 interface under humid conditions, has a low melting point and can function as a liquid phase for ion conduction.[34] However, the liquid phase of $CsH_5(PO_4)_2$ also leads to low mechanical stability of the electrolyte, as reported by Fujiwara *et al.*[36] During the water-splitting test using the CsH_2PO_4/SiP_2O_7 electrolyte, the generated $CsH_5(PO_4)_2$ migrated out of the electrolyte, resulting in electrode corrosion. Wang *et al.* explored the phase diagram of the $(1-x)CsH_2PO_4$–$xCsH_5(PO_4)_2$, revealing the relationship between electrolyte composition and the application temperature range.[37]

Recent studies suggest that LiH_2PO_4 potentially serves as an electrolyte over a broad temperature range.[38] This compound has received less attention as a proton-conductive electrolyte for a long time compared to solid acids, such as CsH_2PO_4 or $CsHSO_4$, due to controversial conductivities reported in the past. In 2008, Lee *et al.* reported that LiH_2PO_4 exhibited high conductivity above 178 °C, around the polymerization temperature of LiH_2PO_4.[39] However, these data have not been reproduced in other reports. In 2021, Berg *et al.* reported that in a closed glass container, LiH_2PO_4 exhibited high conductivity, which potentially introduced a high water vapor pressure to the electrolyte (2 bar at 200 °C).[38] LiH_2PO_4 showed high conductivity even down to room temperature after a melting treatment exceeding 210 °C. The authors noted that achieving high conductivity in LiH_2PO_4 was not possible in an open atmosphere. They concluded that the presence of a high water vapor pressure (*e.g.*, 2 bar at 200 °C) and the process of polymerization after melting were potentially critical to achieving high conductivity in LiH_2PO_4. This stringent preparation protocol, which involves special experimental setups and conditions, makes it difficult for many researchers to access.

In this study, a polymerization-hydrolysis synthesis method was developed to create a self-standing H_3PO_4-LiH_2PO_4/quartz fiber (QF) membrane with high ionic conductivity over a broad temperature range (100–200 °C) under atmospheric pressure. Several control experiments and characterizations were performed to identify the core components for achieving high conductivity. It was found that H_2O vapor, additional H_3PO_4, and the polymerization-hydrolysis procedure were essential for the LiH_2PO_4-based electrolyte to exhibit high conductivity. A highly conductive phase containing H_2O and H_3PO_4 is expected to stabilize on the surface of the LiH_2PO_4 crystalline grains. The presence of a glassy hydrogel intermediate during electrolyte membrane fabrication facilitates the ease of reshaping the process, allowing the production of large-area membranes and highlighting the scalability of this synthetic approach.

Experimental

Materials

Lithium dihydrogen phosphate (≥99%) and phosphoric acid (≥85 wt% in H_2O) were procured from Sigma-Aldrich. A Pt mesh (Φ 0.08 × 50 × 50 mm, 80 mesh, 99.95%) along with a Pt wire (Φ 0.30 mm, 99.95%) were obtained from Nilaco Corporation. QF membranes (with a thickness of 0.38 mm, 85 g cm^{-2}, and Φ 20 mm or 100 mm) were bought from Advantec.

Electrolyte preparation

To prepare the H_3PO_4-LiH_2PO_4/QF electrolyte, LiH_2PO_4 (3 g) was combined with H_3PO_4 in varying stoichiometries (x%H_3PO_4-LiH_2PO_4, where x% represents the molar percentage of phosphoric acid in all the phosphate species, with $x = 0, 3, 9, 15, 21$). This mixture was then heated at 250 °C for 20 min. After the temperature was reduced, a transparent glass was formed. H_2O (1.36 g) was added to the glass. Over 1–2 days, the glass fully dissolved in the water, forming a transparent, viscous hydrosol. Subsequently, the QF membrane was soaked in a hydrosol at a temperature of 60 °C. After emergence, it was removed and then vacuum dried at 60 °C for 2 h. For the LiH_2PO_4/QF sample not treated with additional H_3PO_4, the vacuum drying time was 4 h at 60 °C. The finished membrane, called the polyphosphate hydrogel/QF, was placed in an electrochemical cell to test its conductivity. This electrolyte required hydrolysis treatment at 110 °C under humid conditions for 2 h to achieve high conductivity. The membrane, post-hydrolysis treatment, was designated 15%H_3PO_4-LiH_2PO_4/QF.

Preparation of 15%H_3PO_4-LiH_2PO_4-wo PH/QF electrolyte: a nearly saturated solution of H_3PO_4 and LiH_2PO_4 was prepared in place of the hydrosol solution, with the following composition: LiH_2PO_4: 3 g; H_3PO_4 (85 wt%): 0.6 g; H_2O: 2 g; molar ratio

of H_3PO_4 to LiH_2PO_4 = 0.15 : 0.85. The QF membrane was dipped into this solution at room temperature, removed, and dried on a heating plate at 120 °C for 2 h. The resulting membrane was named 15%H_3PO_4-LiH_2PO_4-wo PH/QF, where "wo PH" denotes "without polymerization–hydrolysis treatment.

Characterization

XRD patterns were obtained using a RINT-Ultima III (Rigaku Corporation) and a Cu Kα X-ray radiation source (λ = 0.154056 nm) at a scan rate of 10° min^{-1}. These diffraction peaks were collected from 10° to 40°. High-resolution field emission SEM (FE-SEM; JEOL; JSM-IT800) with a secondary electron detector was used to obtain the SEM images. TG-DTA8122 (Rigaku Corporation) was used to conduct thermogravimetry and differential thermal analysis (TG-DTA). In these tests, approximately 30 mg of the sample was placed in an aluminum pan, and the weight transition of the sample was monitored as it was heated to 300 °C at a ramping rate of 0.2 °C min^{-1}. These measurements were performed in an air atmosphere. For TG measurement, an Ar gas stream was directed through a room-temperature bubbler for humidification (pH_2O = 3 kPa). Characterization of the phosphate species in the electrolyte was achieved through solid-state ^{31}P magic angle spinning (MAS) NMR spectroscopy. All NMR spectra were collected using a JEOL spectrometer at a Larmor frequency of 200.43 MHz with a laser MAS probe at a spin rate of 15 kHz. Powder samples were packed into a 4-mm insert, which was loaded into a 7-mm rotor and placed into the probe. A single π/2-pulse of 3.25 μs was applied with a recycle delay of 8 s. The ^{31}P NMR shifts were calibrated using $(NH_4)_2HPO_4$ with a ^{31}P resonance at 1.3 ppm. The concentration of phosphates in the precursor solutions and the phosphate salt loading amounts in the membranes were measured using Inductively Coupled Plasma Optical Emission Spectroscopy (ICP-OES) (iCAP PRO XP ICP-OES, Thermo Fisher). 100 μL of the electrolyte precursor solution (comprising both hydrosol and aqueous solution) was diluted 250 000 times in ultrapure water. For the electrolyte salts in the membranes, they were dissolved in 100 mL of ultrapure water before being diluted 500 times.

Measurement of conductivity

The resistance of the electrolyte, R, was determined using electrochemical impedance spectroscopy with a potentiostat system (VMP3; BioLogic Science Instruments). The applicable frequency ranged from 0.1 Hz to 1 MHz, employing a voltage amplitude of 30 mV. Pt meshes with an area of 0.785 cm^2 were utilized as electrodes. R was derived from the high-frequency intercept with the x-axis from the semi-circles and/or linear spikes observed in the Nyquist plots. The conductivity, σ, was then calculated using $\sigma = (1/R) \times (d/A)$, where d and A represent the thickness and area of the electrode, respectively. The thickness of the electrolyte was gauged using a vernier caliper. Impedance spectra were gathered at temperatures ranging from 100 °C to 220 °C within a flowing Ar atmosphere (20 mL min^{-1}). Humidification was attained by applying two methods before insertion into the electrochemical cell (Fig. S1†). To achieve a water vapor pressure below 64 kPa, the Ar stream was directed through a bubbler maintained at temperatures varying from 25 °C to 79 °C. For water vapor pressure ranging from 64 kPa to 87 kPa, the Ar stream was channeled through a vapor tank located in an oven at 110 °C. Liquid H_2O, at a pumping rate of 0.02–0.08 mL min^{-1}, was introduced into the tank, where it was mixed with the Ar stream and water vapor. Water vapor pressure was estimated based on the flow rates of Ar and liquid H_2O, under the presumption of adherence to the ideal gas law. The samples were maintained under each measurement condition, with variations in temperature or humidity, for a duration ranging from 30 min to 24 h before impedance was recorded.

The activation energy of the electrolyte was calculated by applying the Arrhenius law:

$$\sigma = \sigma_0 \exp\left(-\frac{E_a}{k_B T}\right)$$

where σ is the conductivity, T is the temperature, σ_0 is the prefactor, E_a is the activation energy, and k_B is the Boltzmann constant.

Results and discussion

Preparation of H_3PO_4-LiH_2PO_4/QF electrolyte using polymerization-hydrolysis treatment

Fig. 1 illustrates the synthesis process of the 15%H_3PO_4-LiH_2PO_4/QF electrolyte using a polymerization-hydrolysis (PH) method. The transformation of phosphate salt is explained step by step in this section. First, a mixture of LiH_2PO_4 and H_3PO_4 is heated to 250 °C. Here, LiH_2PO_4 melts and polymerization reactions take place in the liquid phase. As shown in Fig. S2,† the TG-DTA analysis of LiH_2PO_4 shows weight loss starting at around 185 °C, followed by a pronounced exothermic peak at 210 °C. Compared to the dehydration study of LiH_2PO_4 reported by Yari *et al.*,[40] the weight loss and the exothermic peak are understood to result from the polymerization (decomposition) and the melting of LiH_2PO_4, respectively. Polymerization is common for all alkali metal dihydrogen phosphates (MH_2PO_4, where M = Li, Na, K, Rb, Cs)[41–43] and is characterized by the following reaction:

$$n\mathrm{MH_2PO_4\ (s)} \rightarrow \mathrm{M}_n\mathrm{H_2P}_n\mathrm{O}_{3n+1}\ \mathrm{(s)} + (n-1)\mathrm{H_2O\ (g)} \quad (1)$$

The polymerization of H_3PO_4 also occurs above 200 °C, forming polyphosphoric acid ($H_{n+2}P_nO_{3n+1}$).[44] At elevated temperatures, H_3PO_4 and LiH_2PO_4 can undergo a mixed polymerization reaction to form a polyphosphate with the chemical formula of $Li_{n-x}H_{2+x}P_nO_{3n+1}$. Upon cooling the molten compound, a transparent glass is formed. The Raman spectra of this glass reveal the presence of monophosphate and various lengths of polyphosphate (as shown in Fig. S3 and Table S1†). It is inferred that the monophosphate phase originates from the residual LiH_2PO_4 and H_3PO_4, which did not fully convert into polyphosphate at 250 °C.

The resulting glass exhibited high hygroscopicity, absorbing water from the air rapidly to form a viscous solution on its

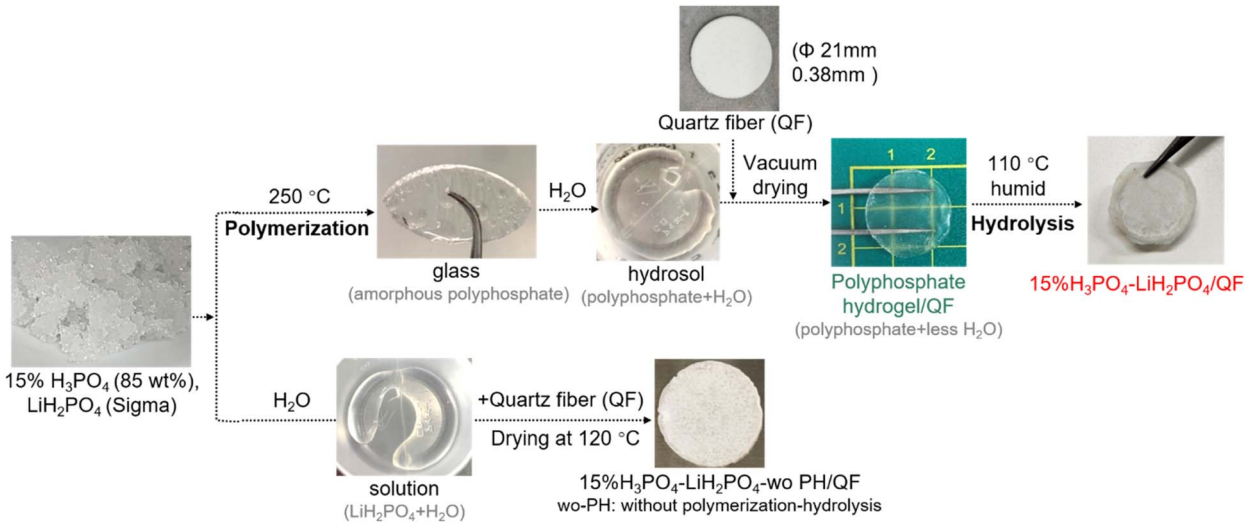

Fig. 1 Fabrication processes of the 15%H_3PO_4-LiH_2PO_4/QF electrolyte and the comparison sample, 15%H_3PO_4-LiH_2PO_4-wo PH/QF electrolyte.

surface. When a regulated quantity of water (1.36 g) was introduced to the glass (3.17 g), the surface dissolved promptly. The complete dissolution of the glass bulk took 1–2 days, which is likely attributed to the slow diffusion rate of water molecules in the polyphosphate. The resultant hydrosol solution is highly viscous at room temperature, rendering the immersion of the quartz fiber (QF) membrane difficult. To assist with the immersion, the membrane and hydrosol were heated to 60 °C. After immersion, the membrane was removed from the hydrosol and vacuum dried at 60 °C for 1–2 h. This step is crucial for decreasing water content and enhancing the membrane's mechanical strength. The resulting membrane, named polyphosphate hydrogel/QF, is transparent and flexible, with a phosphate salt/H_2O weight ratio of around 3.94 (as discussed in Table S2†). *Ex situ* Raman confirmed that the polyphosphate phase remained unchanged during these treatments (polyphosphate glass, polyphosphate hydrosol, and polyphosphate hydrogel/QF in Fig. S3†).

A hydrolysis treatment at 110 °C under humid conditions was necessary for the polyphosphate hydrogel/QF membrane to achieve high conductivity. The membrane, with a diameter of 20 mm and a thickness of 0.6 mm, was placed in an electrochemical cell where the conductivity could be measured (Fig. S1†). Platinum meshes were used as the electrodes, and good contact between the electrodes and the electrolyte was ensured by the pressure of a spring in the cell. As shown in Fig. 2a, the electrolyte's conductivity gradually increased and stabilized at a high value at 110 °C and a partial pressure of water vapor (pH_2O) of 64 kPa. The X-ray diffraction (XRD) pattern of the polyphosphate hydrogel/QF before hydrolysis treatment showed a broad peak, indicating that the polyphosphate phase was amorphous (Fig. 2b). After 3.5 h of treatment at 110 °C and pH_2O of 64 kPa, the XRD pattern revealed the formation of LiH_2PO_4, indicating a transformation of the polyphosphate to monophosphate, as represented by the following reaction:

$$Li_nH_2P_nO_{3n+1}\ (s) + (n-1)H_2O\ (g) \rightarrow nLiH_2PO_4\ (s) \quad (2)$$

The membrane was named 15%H_3PO_4-LiH_2PO_4/QF after the hydrolysis test. The scanning electron microscope (SEM) image of this membrane is shown in Fig. S4.† To investigate the hydrolysis behavior of polyphosphate in more detail, an *in situ* Raman test was performed on the polyphosphate hydrogel/QF membrane in open air (Fig. 2c). The test results demonstrated that the amount of residual water in the membrane was sufficient to hydrolyze a portion of the polyphosphate. At 25 °C, before elevating the temperature, the membrane showed two broad peaks around 720 and 1120 cm^{-1}, which corresponded to the polyphosphate chains of varying lengths.[45] When the temperature increased to 100 °C, the peak indicating the polyphosphate phase decreased, while the monophosphate peak (around 900 cm^{-1}) increased. When the temperature reached 120 °C, the polyphosphate peaks vanished, and the monophosphate peak was similar to that of commercial LiH_2PO_4.[46] These findings suggest that the hydrolysis of lithium polyphosphate to LiH_2PO_4 began at around 100 °C and was fully completed by 120 °C. The thermogravimetric analysis-differential thermal analysis (TG-DTA) data for the polyphosphate hydrogel/QF membrane showed an exothermic peak near 97 °C, which can be attributed to the onset of the hydrolysis reaction (Fig. 2d). The endothermic peak near 140 °C is probably related to the dehydration of polyphosphate compounds that did not entirely convert to monophosphate at lower temperatures (97–140 °C) owing to a lack of water content.

To elucidate the role of polymerization, we prepared an electrolyte named 15%H_3PO_4-LiH_2PO_4-wo PH/QF using a near-saturated solution (containing LiH_2PO_4 and H_3PO_4) without PH treatment (Fig. 1). Table 1 illustrates a comparison between the P concentration in the precursor solutions, the P loading in the membranes, and the resulting conductivities. The P concentration in the hydrosol surpassed that in the saturated

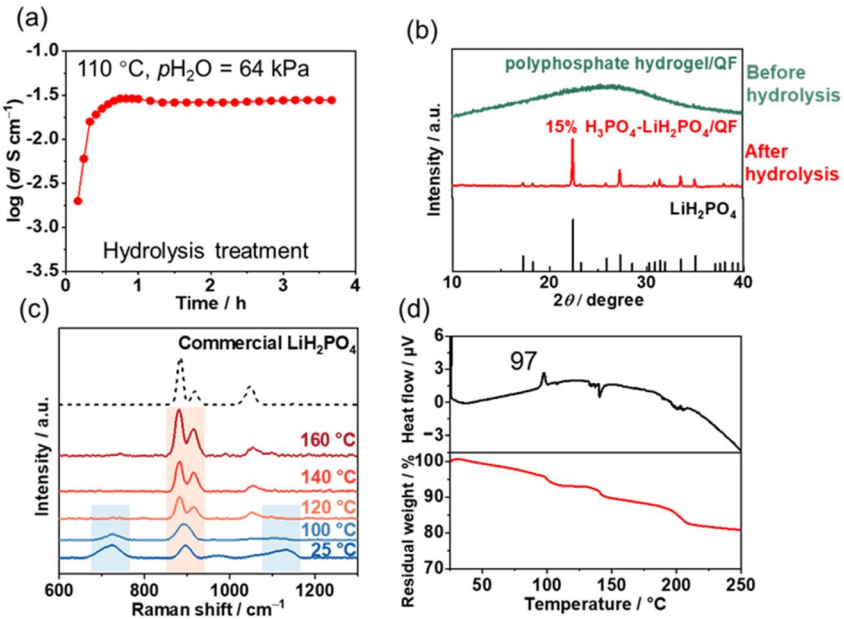

Fig. 2 (a) Conductivity improvement during the hydrolysis of polyphosphate hydrogel/QF at 110 °C, pH_2O = 64 kPa. (b) XRD of polyphosphate hydrogel/QF before and after the hydrolysis treatment. (c) *In situ* Raman of polyphosphate hydrogel/QF. The spectra were collected after stabilizing at each temperature for 30 min. (d) TG-DTA of polyphosphate hydrogel/QF heated at 0.2 °C min^{-1} in air.

Table 1 P concentration in the precursor solutions and its loading on the membranes estimated from ICP-OES, and the conductivity of the membranes at 110 °C and pH_2O = 64 kPa

Precursor solution	Nearly saturated solution	Hydrosol
P concentration/mol L^{-1}	18	26
Membrane	15%H_3PO_4-LiH_2PO_4-wo PH/QF	15%H_3PO_4-LiH_2PO_4/QF
P loading/mg cm^{-2}	13	26
Conductivity/mS cm^{-1} (at 110 °C)	5	28

solution. Consequently, a higher phosphate loading can be achieved in the 15%H_3PO_4-LiH_2PO_4/QF membrane than in 15% H_3PO_4-LiH_2PO_4-wo PH/QF, which contributes to enhanced conductivity.

To clarify the role of the QF membrane in the electrolyte, we attempted to prepare a hydrogel electrolyte sample without the QF support by directly vacuum-drying a small amount of hydrosol. However, the resulting hydrogel sample exhibited poor mechanical stability and was unable to withstand the pressure applied by the current conductivity measurement setup. During the conductivity test, the sample deformed, and a short circuit occurred. A detailed discussion is shown in Fig. S5.† This highlights the critical role of the QF membrane in providing sufficient mechanical strength for the self-supporting electrolyte.

Attempts to synthesize similar membranes using other alkali metal hydrogen phosphates, such as NaH_2PO_4, were unsuccessful because the hydrosol solution could not be successfully prepared using sodium phosphate salt. After the initial polymerization process, the sodium phosphate compound appeared white and opaque, contrasting with the transparent look of lithium phosphate glass (Fig. S6a†). Unlike the lithium phosphate glass compound, this sodium phosphate compound could not be uniformly mixed with a small amount of water (Fig. S6b†). The XRD pattern in Fig. S6c† demonstrated a broad amorphous feature of the lithium phosphate glass, whereas the sodium phosphate compound presented crystalline $Na_2H_2P_2O_7$. The presence of crystalline $Na_2H_2P_2O_7$ may explain the difficulty of forming a highly concentrated solution with sodium phosphate salt owing to the low solubility of $Na_2H_2P_2O_7$ (13 g/100 g H_2O at 20 °C).[47]

Temperature and humidity dependence on phase transformation and conductivity

The application conditions of the developed electrolyte were clarified by conducting conductivity tests under varying temperatures and humidities. As shown in Fig. 3a, the stability test of the 15%H_3PO_4-LiH_2PO_4/QF electrolyte at varying temperatures revealed that at 120 °C and 180 °C, the conductivity of the electrolyte remained stable. However, when the temperature was increased to 200 °C and beyond, the conductivity began to decrease gradually. The XRD pattern of the electrolyte after stability testing at 120 °C and 180 °C confirmed the presence of the LiH_2PO_4 phase, indicating that LiH_2PO_4 phase remained stable up to 180 °C (Fig. 3b). However, the XRD pattern of the electrolyte after the test at 200 °C resembled that of lithium pyrophosphate ($Li_4P_2O_7$). Some subtle differences compared with the peaks of the $Li_4P_2O_7$ reference were

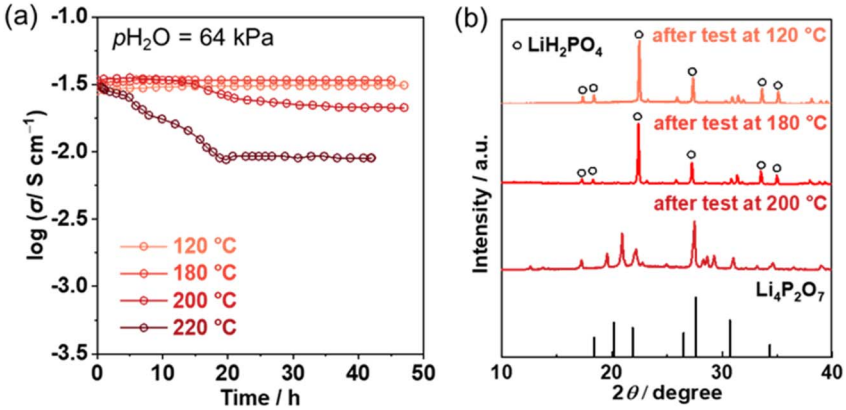

Fig. 3 (a) Stability tests for the 15%H_3PO_4-LiH_2PO_4/QF electrolyte at different temperatures, pH_2O = 64 kPa. All tests were performed after the 3 h of hydrolysis process on the fresh polyphosphate hydrogel/QF electrolytes at 110 °C and pH_2O = 64 kPa (as shown in Fig. 2a). (b) XRD of 15% H_3PO_4-LiH_2PO_4/QF electrolytes after stability tests at different temperatures.

noticeable most probably because a lithium pyrophosphate phase contained additional protons, possibly $Li_2H_2P_2O_7$. It is suggested that the formation of the pyrophosphate phase could result in reduced conductivity. Since the polymerization of LiH_2PO_4 occurs at around 200 °C (as indicated by the endothermic peak in Fig. 2d) and accelerates at higher temperatures,[40] the effective application temperature to maintain the high conductivity of the 15%H_3PO_4-LiH_2PO_4/QF electrolyte is restricted to 200 °C.

The electrolyte conductivity was measured under various humidity levels. Fig. 4a depicts the reversibility test of conductivity at 120 °C with varying pH_2O. The electrolyte demonstrated stable performance under both 64 kPa and 3 kPa pH_2O, with higher conductivity observed at 64 kPa. However, when the vapor pressure was adjusted to 0 kPa, the conductivity started to diminish, thus implying that humidity is essential for maintaining high conductivity in the electrolyte. Upon the reintroduction of vapor, the electrolyte's conductivity started to gradually revive to its original value. Furthermore, recovery was quicker under a higher pH_2O (64 kPa) as opposed to a lower pH_2O (3 kPa). For the conductivity test under pH_2O = 64 kPa, the temperature was further increased to 180 °C to evaluate the electrolyte's stability. As shown in Fig. S7,† the electrolyte exhibited good stability.

Thermogravimetric (TG) testing was performed on the 15% H_3PO_4-LiH_2PO_4/QF electrolyte under humid and dry conditions (Fig. 4b). Owing to experimental constraints, only a low vapor pressure (3 kPa) was applied to the electrolyte to simulate a humid condition. At 3 kPa pH_2O, the electrolyte initially lost weight because it had absorbed a large amount of water from the air owing to its high hygroscopic nature. After the vapor supply was halted after 4.5 h, the electrolyte began losing weight gradually. When 3 kPa of vapor pressure was reintroduced after 22.5 h, the weight of the electrolyte incrementally increased. The weight variations in the electrolyte under humid and dry conditions align with the electrolyte's conductivity changes. Fig. 4c illustrates that the conductivity of 15%H_3PO_4-LiH_2PO_4/QF increased as pH_2O increased. These findings stress the pivotal role of water vapor in obtaining high conductivity in the 15%H_3PO_4-LiH_2PO_4/QF electrolyte.

The importance of H_2O for the conductivity of LiH_2PO_4 was reported by Kweon *et al.* in 2014.[48] Based on MAS nuclear magnetic resonance (NMR) characterizations, the authors concluded that the conductivity of LiH_2PO_4 under humid

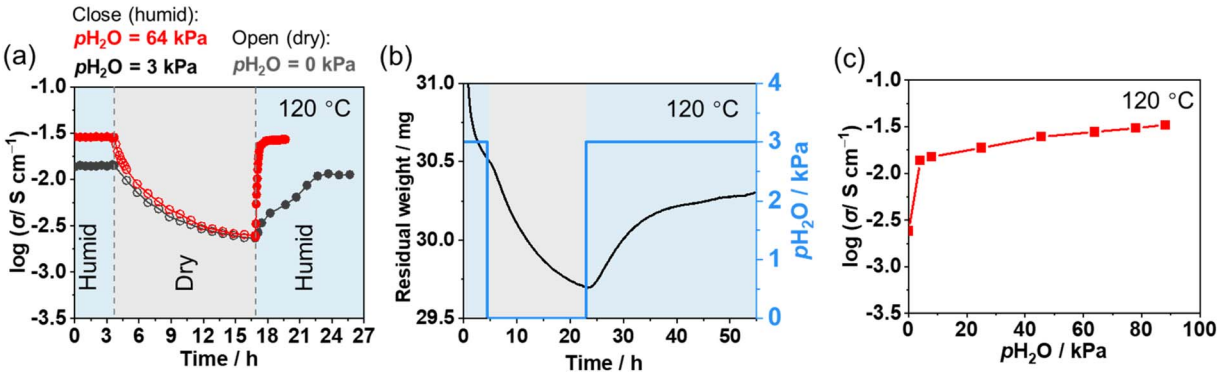

Fig. 4 (a) Reversibility test of the 15%H_3PO_4-LiH_2PO_4/QF between humid conditions (pH_2O = 3 or 64 kPa) and dry conditions (pH_2O = 0 kPa) at 120 °C. (b) TG test of 15%H_3PO_4-LiH_2PO_4/QF between pH_2O = 3 kPa and pH_2O = 0 kPa condition at 120 °C. (c) Conductivity test of 15%H_3PO_4-LiH_2PO_4/QF under different pH_2O at 120 °C. The data points were obtained after the stabilization (1–12 h) at a given pH_2O.

conditions does not stem from proton hopping within the LiH_2PO_4 crystal. Instead, it originates from the rapid exchange between protons in the LiH_2PO_4 crystal and the water molecules absorbed on the LiH_2PO_4 surface. This results in H_3O^+ and proton defects in the crystals. Therefore, the conductivity of LiH_2PO_4 strongly depends on humidity. In this study, TG testing confirmed the strong hygroscopicity of the 15%H_3PO_4-LiH_2PO_4/QF electrolyte, which can absorb water even above 100 °C. This may explain the high conductivity of the electrolyte observed over a wide temperature range (100–200 °C).

H_3PO_4 optimization to improve conductivity

The H_3PO_4 doping amount was optimized in the x%H_3PO_4-LiH_2PO_4/QF electrolyte in our study. As illustrated in Fig. 5a, the conductivity increased with the increase in H_3PO_4 addition, reaching a peak with a doping amount of 15%. The samples with varying H_3PO_4 doping levels exhibited different temperature-dependent behaviors. The conductivity of LiH_2PO_4/QF decreased as the temperature increased, while that of 15%H_3PO_4-LiH_2PO_4/QF increased as the temperature increased. It is inferred that in LiH_2PO_4/QF, the water content may play an essential role in determining conductivity. Elevating the temperature reduces the water content in the electrolyte, which leads to a drop in conductivity. In contrast, the conductivity of 15%H_3PO_4-LiH_2PO_4/QF demonstrated a positive temperature dependence similar to that of pure liquid H_3PO_4,[49] suggesting that the excess H_3PO_4 may have contributed to the high conductivity.

Fig. 5b presents the ^{31}P MAS NMR evaluations for 15% H_3PO_4-LiH_2PO_4/QF, LiH_2PO_4/QF, and commercial LiH_2PO_4. All samples displayed a primary peak at −2.05 ppm, aligning with the phosphorus in the LiH_2PO_4 crystal formation. The consistency in peak positions indicates that the LiH_2PO_4 phase in 15% H_3PO_4-LiH_2PO_4/QF and LiH_2PO_4/QF remains constant, which correlates with the XRD and Raman results (Fig. 2c, 3b, and S8†). In the 15%H_3PO_4-LiH_2PO_4/QF sample, a distinct broad peak is noticeable around 0 ppm, which is attributable to the phosphorus in H_3PO_4.[49] For LiH_2PO_4/QF, compared to the commercial LiH_2PO_4 sample, a slight shoulder appeared above 0 ppm likely owing to the residual H_3PO_4 created during the PH operation. Fig. 5c and d show SEM images of the 15%H_3PO_4-LiH_2PO_4/QF and LiH_2PO_4/QF samples, respectively. The granular particles correspond to LiH_2PO_4 crystals, while the rod-like structures are identified as quartz fibers (Fig. S9†). Additionally, low-magnification SEM tests were conducted at different sites on both samples (Fig. S10†). The 15%H_3PO_4-LiH_2PO_4/QF electrolyte exhibited a relatively continuous and smooth surface, while the LiH_2PO_4/QF sample showed a clearly particulate surface morphology. Given that the NMR results revealed the coexistence of LiH_2PO_4 and H_3PO_4 in the 15%H_3PO_4-LiH_2PO_4/QF sample, it is speculated that H_3PO_4 resides in the interstitial spaces between LiH_2PO_4 particles. This may account for the more continuous and smoother appearance observed in the 15%H_3PO_4-LiH_2PO_4/QF electrolyte.

It is noteworthy that the stabilization of H_3PO_4 on the LiH_2PO_4 surface is a characteristic unique to LiH_2PO_4 among all alkali metal dihydrogen phosphates (MH_2PO_4, M = Cs, Rb, K, Na). Other MH_2PO_4 compounds can react with H_3PO_4 and generate $MH_5(PO_4)_2$.[50] For instance, when H_3PO_4 is doped into CsH_2PO_4, it forms $CsH_5(PO_4)_2$, which melts at 150 °C. Above this temperature, the liquid $CsH_5(PO_4)_2$ contributes to high conductivity, but below 150 °C, solidified $CsH_5(PO_4)_2$ loses its conductivity. Conversely, LiH_2PO_4 and H_3PO_4 do not create $LiH_5(PO_4)_2$. This behavior may be related to the ionic size of Li^+. Compared to the larger ionic radius of Cs^+, the smaller Li^+ ion with higher polarization may be unable to support a crystal structure similar to $CsH_5(PO_4)_2$. Relevant discussions and data are provided in the ESI (Table S3).†

Discussion on the high proton conductivity of the LiH_2PO_4-based electrolyte

Fig. 6a demonstrates a comparison of the conductivity of the electrolyte developed in this study with other electrolytes mentioned in the literature. When compared to commonly studied materials, such as the CsH_2PO_4/SiP_2O_7 solid acid composite and H_3PO_4 doped polymer (PA-PBI), the 15%H_3PO_4-

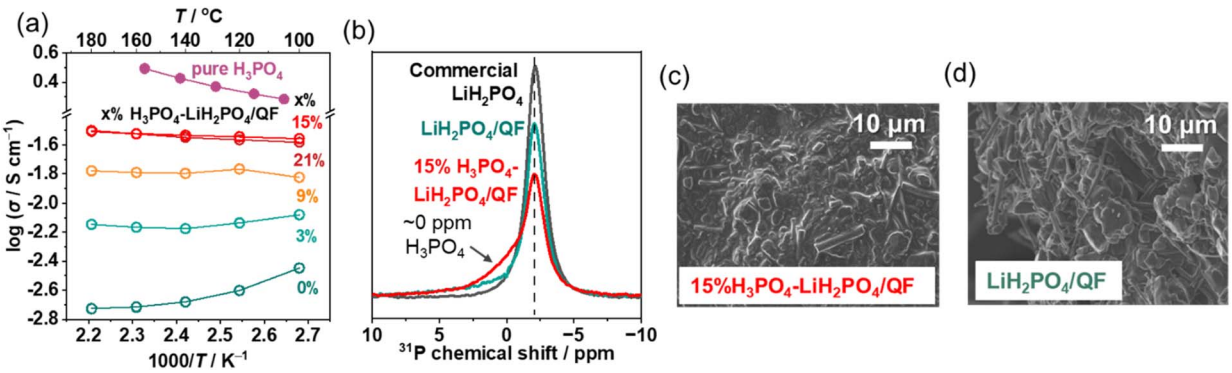

Fig. 5 (a) Conductivity test of LiH_2PO_4/QF with different H_3PO_4 doping amounts under different temperatures, pH_2O = 64 kPa. The conductivity data of pure H_3PO_4 were collected from the study reported by Melchior *et al.*[49] The data points were obtained after stabilization (0.5–1 h) at given temperatures. (b) ^{31}P MAS NMR of 15%H_3PO_4-LiH_2PO_4/QF, LiH_2PO_4/QF, and commercial LiH_2PO_4. (c and d) SEM images of 15%H_3PO_4-LiH_2PO_4/QF and LiH_2PO_4/QF.

LiH_2PO_4/QF electrolyte attains a higher conductivity below 200 °C. A more comprehensive comparison with various types of intermediate temperature solid electrolytes is presented in the ESI (Table S4 and Fig. S11).† Based on the previously mentioned discussion, it can be inferred that the coexistence of H_2O and H_3PO_4 on the LiH_2PO_4 particle surface contributes to high electrolyte conductivity over a broad temperature range. Compared to the activation energy of 0.165 eV for pure liquid H_3PO_4,[49] the 15%H_3PO_4-LiH_2PO_4/QF electrolyte exhibits a significantly lower activation energy of 0.057 eV. Owing to the high hygroscopicity of the 15%H_3PO_4-LiH_2PO_4/QF electrolyte, it absorbs water from the atmosphere at temperatures above 100 °C, potentially leading to low activation energy for proton conduction. As reported by Melchior *et al.*, the combination of H_2O and H_3PO_4 has a lower activation energy than pure H_3PO_4.[49] In contrast to commercial LiH_2PO_4, the 15%H_3PO_4-LiH_2PO_4/QF electrolyte shows greater hygroscopicity, as the electrolyte progressively absorbs water and partially transforms into aqueous solutions under ambient conditions, while the commercial equivalent remains unchanged (Fig. S12†). This difference may be attributed to the smaller particle size of LiH_2PO_4 in the 15%H_3PO_4-LiH_2PO_4/QF electrolyte (Fig. S9a and b†) and differences in hydrogen bonding, as revealed by Raman spectra (Fig. S9c†).

The conductivity of LiH_2PO_4 has previously been a subject of debate. This discrepancy, according to the present study, could potentially arise from the water content in the electrolyte pellet, the water vapor pressure, and the pretreatment methods used in different experimental processes. For instance, previous studies by Lee *et al.* and Urtiaga evaluated the conductivity of LiH_2PO_4 pellets made of polycrystalline powder under low humidity conditions (Table 2 and Fig. 6a).[39,51] Moreover, although Urtiaga preheated the LiH_2PO_4 at 80 °C in the air for 24 h to lessen the remaining water in the electrolyte before measuring conductivity,[51] Lee *et al.* did not pretreat the synthesized LiH_2PO_4.[39] Considering the high hygroscopic nature of LiH_2PO_4 reported by Lee *et al.*, it is postulated that water could be absorbed onto the surface of LiH_2PO_4 particles, influencing its conductivity.[48] Uniquely, Berg *et al.* performed the conductivity measurements inside a sealed glass container capable of maintaining high water vapor pressure (*e.g.*, pH_2O = 2 bar at 200 °C).[38] They observed a decrease in conductivity when the tests were conducted in the open air. Although both the aforementioned studies took measurements from low to high temperatures, Berg *et al.*'s measurements started at a high temperature of 272 °C,[38] which is above both the polymerization and melting temperatures. All the previous studies were conducted on LiH_2PO_4 alone to clarify its function. Our study demonstrates the high conductivity of H_3PO_4 and LiH_2PO_4 over a broad temperature range after polymerization and hydrolysis treatment. Conductivity tests conducted under various humidity conditions have shed light on the high conductivity of LiH_2PO_4-based electrolytes. Compared to Berg *et al.*'s study, the inclusion of H_3PO_4 permits LiH_2PO_4 electrolytes to exhibit high conductivity under ambient pressure, considerably enhancing their prospective application in electrochemical devices.

Scalability and practical application of electrolyte membranes

To illustrate the scalability of the PH synthesis process, the diameter of the QF membrane was increased from 2 cm to 10 cm. As depicted in Fig. 6b, different portions of the membrane were sliced, and their conductivities were evaluated at 120 and 160 °C after undergoing hydrolysis treatment at 110 °C (Fig. 6c). The findings were akin to those of the smaller 2 cm diameter membrane, signifying the scalability of the current method. Both membranes with different sizes exhibited sufficient mechanical strength to be handled easily, as shown in Fig. S13.†

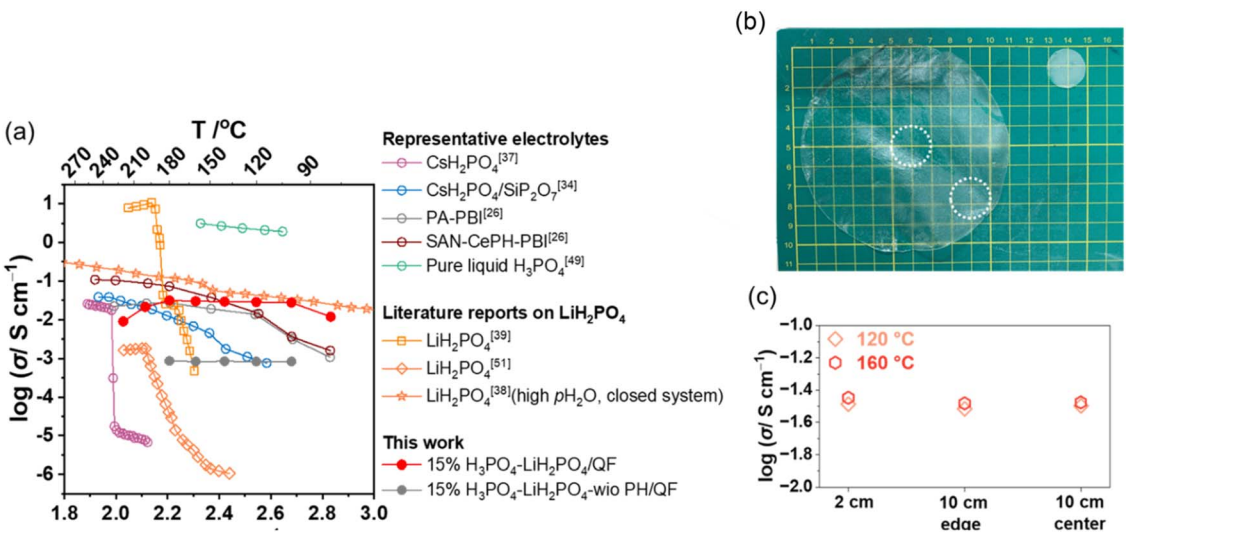

Fig. 6 (a) A comparison of the conductivity of electrolytes in this work with representative electrolytes[26,34,37,49] at intermediate temperatures and previous reports on the conductivity of LiH_2PO_4.[38,39,51] (b) Images of polyphosphate hydrogel/QF with diameters of 2 and 10 cm. The regions selected for the conductivity tests are shown as dashed circles in the sample with a 10 cm diameter. (c) Conductivity comparison of electrolyte membranes with diameters of 2 and 10 cm at pH_2O = 64 kPa. The data points were obtained after stabilization (0.5–1 h) at given temperatures.

Table 2 Comparison of experimental conditions for the conductivity test of LiH_2PO_4 in previous reports[a]

Ref.	LiH_2PO_4 sample status	Humid condition	Measurement direction	Additional information
39	Pellet prepared by grinding LiH_2PO_4 powder	Low humidity atmosphere (open air?)	40 °C → 226 °C	
51	Pellet prepared by grinding LiH_2PO_4 powder	Relative humidity = 3.0%	125 °C → 220 °C	LiH_2PO_4 was heated at 80 °C for 24 h before pressing into a pellet
38	Untreated commercial LiH_2PO_4	Changed with temperature (*e.g.*, pH_2O = 2 bar at 200 °C)	272 °C → 359 °C → 32 °C	The sample was loaded in a closed glass container
This study	15%H_3PO_4-LiH_2PO_4/QF membrane	pH_2O = 4–98 kPa	100 °C → 180 °C	

[a] LiH_2PO_4 polymerization temperature: ~180 °C; melting temperature: ~210 °C.

To evaluate the practical applicability of the electrolyte membrane, steam electrolysis tests were conducted in an intermediate temperature electrochemical cell (Fig. S14†). After optimizing the ambient humidity conditions, stable cell operation was achieved, with a faradaic efficiency for hydrogen generation of approximately 90% (Fig. S15†). However, the stable operation of the electrolyte is limited to relatively low temperatures (110 °C). The experimental results are discussed in the ESI.† Future work will focus on optimizing the structure and composition of the electrolyte matrix materials, with reference to similar electrolytes to gain further insights.[52–55] It is expected that by enhancing the water retention ability of the electrolyte, the operational performance of the electrolyte can be improved across a broader temperature range.

Conclusions

In summary, an H_3PO_4-LiH_2PO_4/QF electrolyte membrane was successfully developed using a unique polymerization-hydrolysis (PH) synthesis method, demonstrating high conductivity over a broad temperature range (100 °C to 200 °C). The key factors that contributed to achieving this high conductivity are as follows: (1) adequate salts embedded in the membrane through PH treatment, (2) the incorporation of extra H_3PO_4, and (3) humid conditions. It is hypothesized that a highly conductive interface forms between the LiH_2PO_4 particles that contain H_3PO_4 and H_2O, contributing significantly to the electrolyte's high conductivity. TG analysis highlighted the electrolyte's high hygroscopicity, which allows it to absorb water from the atmosphere at temperatures exceeding 100 °C. This property likely explains its consistent conductivity performance over a wide temperature range compared to other intermediate-temperature electrolytes. The PH synthesis process also showed scalability, enabling the production of larger membranes by simply adjusting the dimensions of the QF membrane. In summary, this study presents a new synthesis method for the LiH_2PO_4 solid acid electrolyte and offers valuable insights into its proton conduction mechanism.

Data availability

Data for this article, including the electrochemical dataset, are available at the Science Data Bank at **https://doi.org/10.57760/sciencedb.27594**.

Author contributions

Ke Xu: conducted most of the experiments and characterizations and wrote the first draft of the manuscript. Keisuke Obata: wrote the manuscript with K. X. and provided daily research supervision. Takaaki Suzuki: supervised the MAS NMR measurements. Kazuya Yamaguchi: review, editing and supervision. Masao Katayama: supervision and review. Kazuhiro Takanabe: review and editing, conceptualization, methodology, funding acquisition, and project administration.

Conflicts of interest

There are no conflicts to declare.

Acknowledgements

This work was based on results obtained from a project commissioned by the New Energy and Industrial Technology Development Organization. This work was also supported by IHI Corporation. The authors acknowledge Prof. Jun Kubota at Fukuoka University for providing information on the high-temperature electrolytic cell and for detailed discussion of the experimental operation.

References

1 S. M. Haile, D. A. Boysen, C. R. I. Chisholm and R. B. Merle, *Nature*, 2001, **410**, 910–913.
2 D. A. Boysen, T. Uda, C. R. I. Chisholm and S. M. Haile, *Science*, 2004, **303**, 68–70.
3 M. Nagao, T. Kamiya, P. Heo, A. Tomita, T. Hibino and M. Sano, *J. Electrochem. Soc.*, 2006, **153**, A1604–A1609.
4 H. Steininger, M. Schuster, K. D. Kreuer, A. Kaltbeitzel, B. Bingöl, W. H. Meyer, S. Schauff, G. Brunklaus, J. Maier and H. W. Spiess, *Phys. Chem. Chem. Phys.*, 2007, **9**, 1764–1773.
5 K. Imamura and J. Kubota, *Sustainable Energy Fuels*, 2019, **3**, 1406.
6 J. Kim, D. Jang, J. Choi, J. Maeng, H. Shin, T. Park and W. Kim, *Catalysts*, 2023, **13**, 707–719.
7 J. Kubota, T. Okumura and R. Hayashi, *Sustainable Energy Fuels*, 2022, **6**, 1362–1372.

8 A. Chandan, M. Hattenberger, A. El-kharouf, S. Du, A. Dhir, V. Self, B. G. Pollet, A. Ingram and W. Bujalski, *J. Power Sources*, 2013, **231**, 264–278.
9 S. M. Haile, H. Liu and R. A. Secco, *Chem. Mater.*, 2003, **15**, 727–736.
10 J. Otomo, N. Minagawa, C.-j. Wen, K. Eguchi and H. Takahashi, *Solid State Ionics*, 2003, **156**, 357–369.
11 D. Aili, J. Zhang, M. T. Dalsgaard Jakobsen, H. Zhu, T. Yang, J. Liu, M. Forsyth, C. Pan, J. O. Jensen, L. N. Cleemann, S. P. Jiang and Q. Li, *J. Mater. Chem. A*, 2016, **4**, 4019–4024.
12 S. Wang, C. Zhao, W. Ma, N. Zhang, Y. Zhang, G. Zhang, Z. Liu and H. Na, *J. Mater. Chem. A*, 2013, **1**, 621–629.
13 K. Genzaki, P. Heo, M. Sano and T. Hibino, *J. Electrochem. Soc.*, 2009, **156**, B806–B810.
14 A. Goñi-Urtiaga, D. Presvytes and K. Scott, *Int. J. Hydrogen Energy*, 2012, **37**, 3358–3372.
15 N. Mohammad, A. B. Mohamad, A. A. H. Kadhum and K. S. Loh, *J. Power Sources*, 2016, **322**, 77–92.
16 G. Kim, J. M. Griffin, F. Blanc, S. M. Haile and C. P. Grey, *J. Am. Chem. Soc.*, 2015, **137**, 3867–3876.
17 C. R. I. Chisholm, R. B. Merle, D. A. Boysen and S. M. Haile, *Chem. Mater.*, 2002, **14**, 3889–3893.
18 F. Romain and A. Novak, *J. Mol. Struct.*, 1991, **263**, 69–74.
19 E. Ortiz, R. A. Vargas and B. E. Mellander, *J. Chem. Phys.*, 1999, **110**, 4847–4853.
20 E. Ortiz, J. Romero Atencio and E. Martínez, *J. Therm. Anal. Calorim.*, 2021, **147**, 3519–3529.
21 E. Ortiz, I. Piñeres and C. León, *J. Therm. Anal. Calorim.*, 2016, **126**, 407–419.
22 J.-H. Park, *Phys. Rev. B: Condens. Matter Mater. Phys.*, 2004, **69**, 054104.
23 L. Xiao, H. Zhang, E. Scanlon, L. S. Ramanathan, E.-W. Choe, D. Rogers, T. Apple and B. C. Benicewicz, *Chem. Mater.*, 2005, **17**, 5328–5333.
24 X. Sun, S. C. Simonsen, T. Norby and A. Chatzitakis, *Membranes*, 2019, **9**, 83.
25 X. Li, H. Ma, P. Wang, Z. Liu, J. Peng, W. Hu, Z. Jiang and B. Liu, *ACS Appl. Mater. Interfaces*, 2019, **11**, 30735–30746.
26 S. Lee, J. G. Seong, Y. Jo, S.-J. Hwang, G. Gwak, Y. Park, Y. C. Kim, K. H. Lim, H.-Y. Park, J. H. Jang, H.-J. Kim, S.-W. Nam and S. Y. Lee, *Nat. Energy*, 2024, **9**, 849–861.
27 O. Paschos, J. Kunze, U. Stimming and F. Maglia, *J. Phys.: Condens. Matter*, 2011, **23**, 234110.
28 M. Nagao, A. Takeuchi, P. Heo, T. Hibino, M. Sano and A. Tomita, *Electrochem. Solid-State Lett.*, 2006, **9**, A105–A109.
29 S. Tao, *Solid State Ionics*, 2009, **180**, 148–153.
30 I. Suzuki, M. Tashiro, T. Yamaguchi, T. Ishiyama, J. Nishii, T. Yamashita, H. Kawazoe and T. Omata, *Int. J. Hydrogen Energy*, 2020, **45**, 16690–16697.
31 T. Omata, A. Sharma, I. Suzuki, T. Ishiyama, S. Kohara, K. Ohara, M. Ono, Y. Ren, K. Zagarzusem, M. Fujioka, G. Zhao and J. Nishii, *ChemPhysChem*, 2022, **23**, e202100840.
32 V. G. Ponomareva and E. S. Shutova, *Solid State Ionics*, 2007, **178**, 729–734.
33 A. H. Jensen, Q. Li, E. Christensen and N. J. Bjerrum, *J. Electrochem. Soc.*, 2014, **161**, F72–F76.
34 T. Matsui, T. Kukino, R. Kikuchi and K. Eguchi, *J. Electrochem. Soc.*, 2006, **153**, A339–A342.
35 V. G. Ponomareva, E. S. Shutova and G. V. Lavrova, *Inorg. Mater.*, 2008, **44**, 1009–1014.
36 N. Fujiwara, H. Nagase, S. Tada and R. Kikuchi, *ChemSusChem*, 2021, **14**, 417–427.
37 L. S. Wang, S. V. Patel, E. Truong, Y.-Y. Hu and S. M. Haile, *Chem. Mater.*, 2022, **34**, 1809–1820.
38 R. W. Berg, A. V. Nikiforov and N. J. Bjerrum, *Ionics*, 2021, **27**, 703.
39 K.-S. Lee, J. Moon, J. Lee and M. Jeon, *Solid State Commun.*, 2008, **147**, 74–77.
40 B. Yari, P. Sauriol and J. Chaouki, *Can. J. Chem. Eng.*, 2019, **97**, 2273–2286.
41 P. Jong-Ho, L. Kwang-Sei and C. Byung-Chun, *J. Phys.: Condens. Matter*, 2001, **13**, 9411–9419.
42 E. Ortiza, R. A. Vargasb and B.-E. Mellanderc, *Solid State Ionics*, 1999, **125**, 177.
43 A. Ghule, R. Murugan and H. Chang, *Inorg. Chem.*, 2001, **40**, 5917–5923.
44 S. Penczek, J. Pretula, P. Kubisa, K. Kaluzynski and R. Szymanski, *Prog. Polym. Sci.*, 2015, **45**, 44–70.
45 T. Yamaguchi, Y. Saito, Y. Kuwahara, H. Yamashita, T. Ishiyama, J. Nishii, T. Yamashita, H. Kawazoe and T. Omata, *J. Mater. Chem. A*, 2017, **5**, 12385–12392.
46 K.-S. Lee, J.-H. Ko, J. Moon, S. Lee and M. Jeon, *Solid State Commun.*, 2008, **145**, 487–492.
47 Y. M. Abd-Elhakim, M. M. Hashem, A. Anwar, A. E. El-Metwally, K. Abo-El-Sooud, G. G. Moustafa, S. M. Mouneir and H. A. Ali, *Environ. Toxicol. Pharmacol.*, 2018, **62**, 98–106.
48 J. J. Kweon, R. Fu, E. Steven, C. E. Lee and N. S. Dalal, *J. Phys. Chem. C*, 2014, **118**, 13387–13393.
49 J.-P. Melchior, K.-D. Kreuer and J. Maier, *Phys. Chem. Chem. Phys.*, 2017, **19**, 587–600.
50 H. Muroyama, K. Kudo, T. Matsui, R. Kikuchi and K. Eguchi, *Solid State Ionics*, 2007, **178**, 1512–1516.
51 A. G. Urtiaga, Doctor thesis, Newcastle University, 2014.
52 J. M. Hu, H. R. Wang, Y. G. Yang, Y. Li and Q. H. Wu, *RSC Adv.*, 2021, **11**, 33858–33866.
53 Y. N. Zhu, C. Y. Liu, Y. G. Yang, Li Yi and Q. H. Wu, *Electrochim. Acta*, 2023, **446**, 142097.
54 X. B. Chen, B. Put, A. Sagara, K. Gandrud, M. Murata, J. A. Steele, H. Yabe, T. Hantschel, M. Roeffaers, M. Tomiyama, H. Arase, Y. Kaneko, M. Shimada, M. Mees and P. M. Vereecken, *Sci. Adv.*, 2020, **6**, eaav3400.
55 S. Ishibe, K. Anzai, J. Nakamura, Y. Konosu, M. Ashizawa, H. Matsumoto and Y. Tominaga, *React. Funct. Polym.*, 2014, **81**, 40–44.